

A Study on Red Asymmetry of $H\alpha$ Flare Ribbons Using Narrowband Filtergram in the 2001 April 10 Solar Flare

Ayumi ASAI¹, Kiyoshi ICHIMOTO² Reizaburo KITAI², Hiroki KUROKAWA², and Kazunari SHIBATA²

¹*Unit of Synergetic Studies for Space, Kyoto University, Yamashina, Kyoto, 607-8471, Japan*
asai@kwasan.kyoto-u.ac.jp

²*Kwasan and Hida Observatory, Kyoto University, Yamashina, Kyoto, 607-8471, Japan*

(Received 2009 July 1; accepted 2011 September 20)

Abstract

We report a detailed examination of the “red asymmetry” of $H\alpha$ emission line seen during the 2001 April 10 solar flare by using a narrowband filtergram. We investigated the temporal evolution and the spatial distribution of the red asymmetry by using the $H\alpha$ data taken with the 60cm Domeless Solar Telescope at Hida Observatory, Kyoto University. We confirmed that the red asymmetry clearly appeared all over the flare ribbons, and the strong red asymmetry is located on the outer narrow edges of the flare ribbons, with the width of about $1.''5 - 3.''0$ (1000 – 2000 km), where the strong energy releases occur. Moreover, we found that the red asymmetry, which also gives a measure of the Doppler shift of the $H\alpha$ emission line concentrates on a certain value, not depending on the intensity of the $H\alpha$ kernels. This implies not only that the temporal evolutions of the red asymmetry and those of the intensity are not in synchronous in each flare kernel, but also that the peak asymmetry (or velocity of the chromospheric condensation) of individual kernel is not a strong function of their peak intensity.

Key words: acceleration of particles — Sun: chromosphere — Sun: corona — Sun: flares

1. Introduction

Solar flares have been extensively observed in $H\alpha$ line, since they show spectacular phenomena in this wavelength, such as filament/prominence eruptions, flare ribbons, post flare loops (or coronal rains), and so on (e.g. Tandberg-Hanssen & Emslie 1988). $H\alpha$ kernels, very bright and compact $H\alpha$ emission sources seen in flare ribbons, are also one of the prominent features that appear during a flare. Such flare ribbons and kernels have been thought to be

caused by the energy deposition from the corona into the chromosphere.

To explain these various phenomena successfully, magnetic reconnection models have been widely discussed for last several decades. Especially, the so-called CSHKP magnetic reconnection model (Carmichael 1964; Sturrock 1966; Hirayama 1974; Kopp & Pneuman 1976) is often accepted as the “standard” model. In the scenario, the connectivity of magnetic field lines is topologically changed (i.e. re-connected) in the corona, and then, vast magnetic energy stored in the corona is released. The released energy is converted to various kinds of energy; kinetic energy spent for ejections of plasma, thermal energy to generate hot plasma of about 10 MK or more, nonthermal energy to accelerate energetic particles, and so on. The thermal conduction and/or the nonthermal particles rapidly travel along newly connected magnetic field lines. Then, they reach the chromosphere, followed by the bombardment to the chromospheric plasma. $H\alpha$ flare ribbons and kernels are caused by such bombardment. The CSHKP model further suggests that magnetic field lines successively reconnect in the corona. During the successive magnetic reconnection, the reconnection points (X-points) move upward. As a result, newly reconnected field lines have their footpoints farther out from the neutral line than the footpoints of the field lines that have already reconnected. Therefore, the separation of the flare ribbons is not a real motion, but an apparent one (see also the reviews of the CSHKP model by Sturrock 1992 and Švestka & Cliver 1992).

The energy deposition into the chromosphere also causes strong distortions of $H\alpha$ line (line width and line shift) besides the emission. The enhancements of the intensity at red wings are particular, and have been reported as “red asymmetry” of the lines (Švestka 1976), while “blue asymmetry” is also reported to be sometimes seen at very early phase of a flare. Comparing between the red and the blue wing images, it has known that such red asymmetry is seen overall the flare ribbons (Janssens & White 1970; Švestka 1976; Tang 1983). Hanaoka (2003) examined the $H\alpha$ impact polarization (liner polarization) due to collisions of high-energy particles at flare kernels, and reported that red asymmetry also appears at such kernels during the rise phase of kernel brightenings. Observations on the red asymmetry with filtergraphs, however, have not been progressed so much since then, and the further characteristics on the spatial distribution of the red asymmetry remains to be revealed.

Ichimoto & Kurokawa (1984) reported that the red-shift corresponds to the downward motion with speed of several tens of km s^{-1} , based on their excellent spectroscopic observations. Falchi et al. (1997) further reported that strong red asymmetry, which corresponds to the downward velocity of the order of tens of km s^{-1} , is observed at the outer edge of the flare ribbons. The width of the edges is about $2 - 3''$ ($\sim 1500 - 2000$ km). This is reasonable in the context of magnetic reconnection theories suggesting that strong energy depositions occur at the outer edges of the flare ribbons connected by the newly reconnected loops. Ichimoto & Kurokawa (1984) also quantitatively examined the red asymmetry. The strong enhancement of the chromospheric plasma due to the precipitation of nonthermal plasma and/or thermal

conduction causes not only red asymmetry of the chromospheric lines but explosive upflow of the heated plasma along the flare loops. The latter is called “chromospheric evaporation”, and has been observed as blue-shift of coronal emission lines (Hirayama 1974; Antonucci et al. 1984). Ichimoto & Kurokawa (1984) found a momentum balance between the downward motion of the chromospheric condensation and the chromospheric evaporation, and confirmed that the red asymmetry is a counteraction of the chromospheric evaporation.

Red asymmetry, in this way, tells us the quantitative information of the precipitation (nonthermal particles / thermal conduction). Understanding the features of the chromospheric plasma at the footpoints of flare loops is strongly related with understanding energy release/deposit mechanisms and is crucially important for solar flare studies. It has been, however, a challenge theoretically and numerically to explain exactly those observational facts (e.g. Fisher et al. 1985a; Fisher et al. 1985b), since the distortion of chromospheric lines is too complicated. Observations on the red asymmetry, have not been progressed so much since Ichimoto & Kurokawa (1984). Especially, spatial distribution of the red asymmetry using narrowband filtergram, remains to be revealed, although Tang (1983) reported that red asymmetry features appear all over flare ribbons and continue from onset until late in the decay phase by using narrowband filtergram of $H\alpha$ line. In this paper we examined the spatial distribution of the red asymmetry at $H\alpha$ kernels and the temporal evolution, by using $H\alpha$ wing images. In § 2 we summarize the observational data and the features of the flare. In § 3 we show the features of the red asymmetry. In § 4 a summary and discussions are given.

2. Observations

We observed a typical two-ribbon flare (X2.3 on the GOES scale) that occurred in the NOAA Active Region 9415 (S22°, W01°) at 05:10 UT, 2001 April 10 with the 60 cm Domeless Solar Telescope (DST¹) at Hida Observatory, Kyoto University. The $H\alpha$ monochromatic images were obtained with the Zeiss Lyot filter of the 0.25 Å passband and KODAK 4.2i Megapixels CCD camera with the size of 2024 × 2040 pixels sequentially in eight wavelengths: $H\alpha$ −1.5, −0.8, −0.4, ±0.0, +0.4, +0.8, +1.5, and +5.0 Å. The successive wavelength change and recording were controlled with a personal computer, and the time cadence for each wavelength was about 30 s. The pixel size of the data is 0."28 (the highest resolution of the system is 0."14, but binning was done in the current case). However, the spatial resolution is about 2" or worse according to the seeing.

In Figure 1 we present snap shots of the $H\alpha$ images in the (a) −1.5, (b) −0.8, (c) −0.4, (d) ±0 (line center), (e) +1.5, (f) +0.8, (g) +0.4, and (h) +5.0 Å wings, respectively. During the observation, the emissions at $H\alpha$ kernels were so strong that some fine structures inside the flare ribbons were missed suffering from the saturation in the core. In this study, therefore, we

¹ http://www.kwasan.kyoto-u.ac.jp/general/facilities/dst/index_en.html

mainly used the $H\alpha$ -1.5 and $+1.5$ Å images only, in which the flare kernels are clearly seen rarely suffering from the saturation. In Figure 2 we show the temporal development of the flare in the $H\alpha$ center (*top*), in the $+0.8$ Å wing (*middle*), and in the -0.8 Å wing (*bottom*). The filament eruption is clearly seen in the blue wing images before the two ribbon flare starts. As the flare progresses the two ribbon structure evolves and separates to each other. In the later phase, downflows along the post flare loops (coronal rains) are also seen in red wing images.

As Figure 1 shows and Asai et al. (2004) reported, the two flare ribbons lie roughly in the north-south direction, and the east (left) ribbon is of positive magnetic polarity, and the west (right) one is of negative polarity. As the flare progresses, the flare ribbons separate to each other, in the horizontal (that is, in the east-west) direction. We already reported the characteristics of the flare in $H\alpha$, which was observed with the *Sartorius* Telescope at Kwasan Observatory, Kyoto University, in some previous papers (Asai et al. 2002; Asai et al. 2003; Asai et al. 2004). We also quantitatively discussed the relation between the flare ribbon evolution and the energy release rate in these papers. Xie et al. (2009) also studied the ribbon separation of this flare. In this event the oscillation of an $H\alpha$ filament driven by an EIT wave is also detected in a distant location (Okamoto et al. 2004).

2.1. Determination of Line Center

Before examining the characteristics of the red asymmetry, we checked the central position of the wavelength scan by the Lyot filter with respect to the averaged $H\alpha$ line center of the target region. Since not only the tuning offset of the filter but also the solar rotation and the motion of the earth can cause a relative offset of the wavelength, we should know how much the line center is shifted during the observation. We used the averaged intensity of a quiet region near the flare site shown with the box in Figure 1 (a), and confirmed that the center of the Lyot filter was $+0.05$ Å displaced from the actual center of the $H\alpha$ absorption. Although such small offset may produces a fictitious shift of the spectral line, it can hardly produce a significant asymmetry of intensity as observed in far wings (such as at ± 1.5 Å) of the emission $H\alpha$ line.

Comparing Figure 1 (a) with (e), we can clearly see that the flare ribbons are much brighter in the $+1.5$ Å wing than in the -1.5 Å wings, and we can conclude that the intensity asymmetry is mainly caused by the effect of the red asymmetry (or red shift) of the $H\alpha$ line. Thus, we neglect the small offset of the observing wavelength in the following discussions.

3. Red Asymmetry

As the pair of the snap shots of Figure 1 (a) and (e) simply but clearly show, most portions of the flare ribbons are brighter in the red-wing (that is, $H\alpha$ $+1.5$ Å) than those in the blue-wing ($H\alpha$ -1.5 Å). This means that red asymmetry appears all over the flare ribbons, not only at bright kernels made by the bombardment of nonthermal particles, but also at other

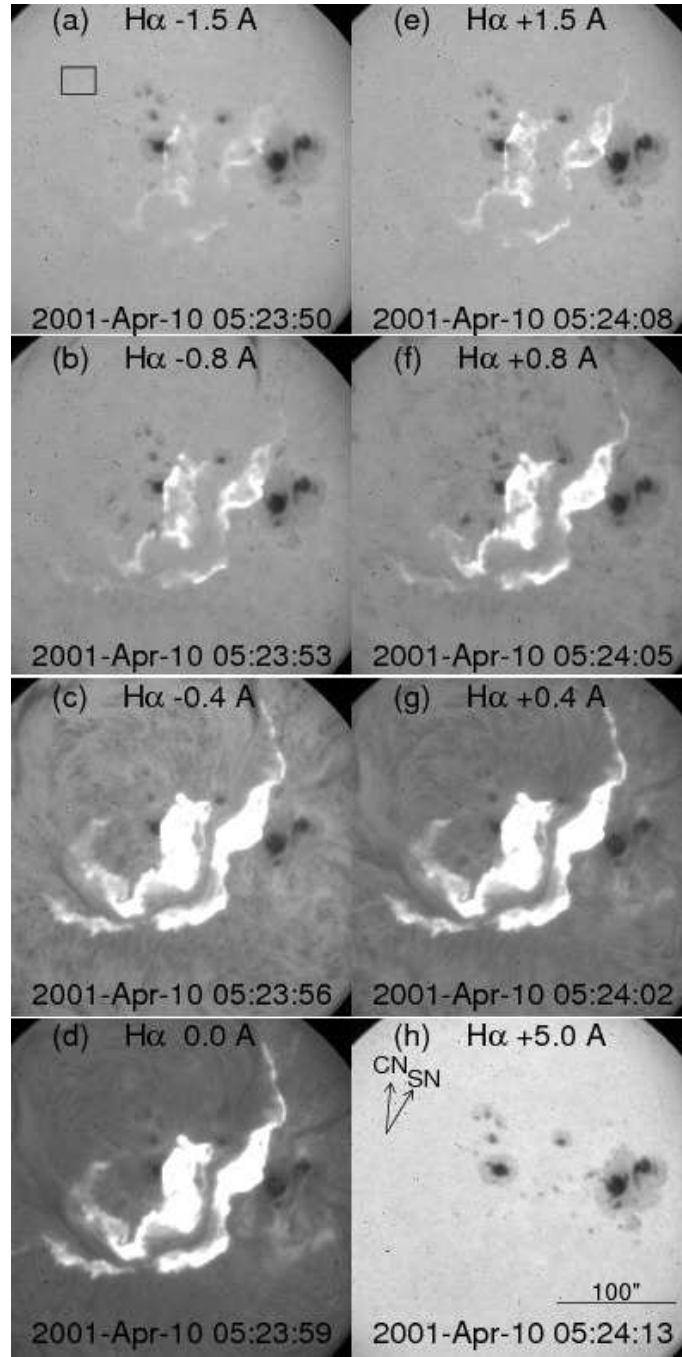


Fig. 1. $H\alpha$ images of the 2001 April 10 flare in the (a) -1.5 , (b) -0.8 , (c) -0.4 , (d) ± 0 (line center), (e) $+1.5$, (f) $+0.8$, (g) $+0.4$, and (h) $+5.0$ \AA wings of $H\alpha$ line. Celestial north is up as shown with the arrow denoted “CN” in the panel (f), and west is to the right. The direction of the solar north is also shown with the arrow denoted “SN” in the panel (h).

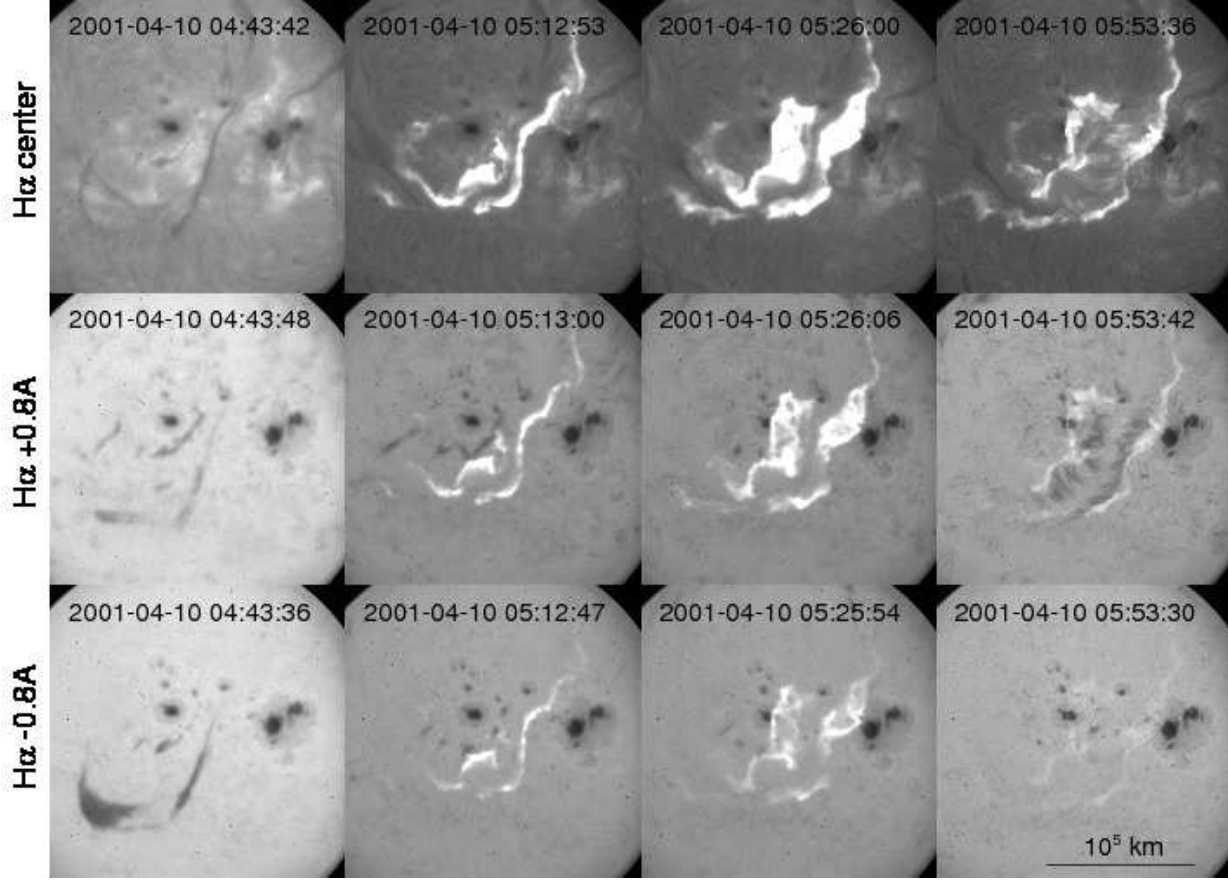


Fig. 2. Temporal evolution of the 2001 April 10 flare in H α line center (*top*), in $+0.8 \text{ \AA}$ (*middle*), and in -0.8 \AA (*bottom*). Celestial north is up, and west is to the right.

fainter points that are likely generated by the thermal conduction.

3.1. Temporal Evolution of RA

The right two panels of Figure 3 show the temporal evolution of the H α intensities in the red ($+1.5 \text{ \AA}$: red line) and blue (-1.5 \AA : blue line) wings for the selected flare kernels marked in the left panel of Figure 3. At these flare kernels, the intensity in the red wing I_{red} is always brighter than that in the blue wing I_{blue} during the burst. As we showed in the previous papers (Asai et al. 2003; Asai et al. 2004), we found nonthermal emissions in hard X-rays and in microwaves observed with the Hard X-ray Telescope (HXT; Kosugi et al. 1991) on board *Yohkoh* (Ogawara et al. 1991) and with the Nobeyama Radioheliograph (NoRH; Nakajima et al. 1994), respectively, at these flare kernels. We also plotted the light curves of the microwave (17 GHz) and the hard X-ray (the H band; 53 – 93 keV) emissions in Figure 3 with the black and gray solid lines. There are several peaks and the positions of the emission sources move during the impulsive phase. The flare kernels \triangle and \times are associated with the nonthermal emission sources whose peak times are 05:19 and 05:22UT, respectively, as colored with vertical

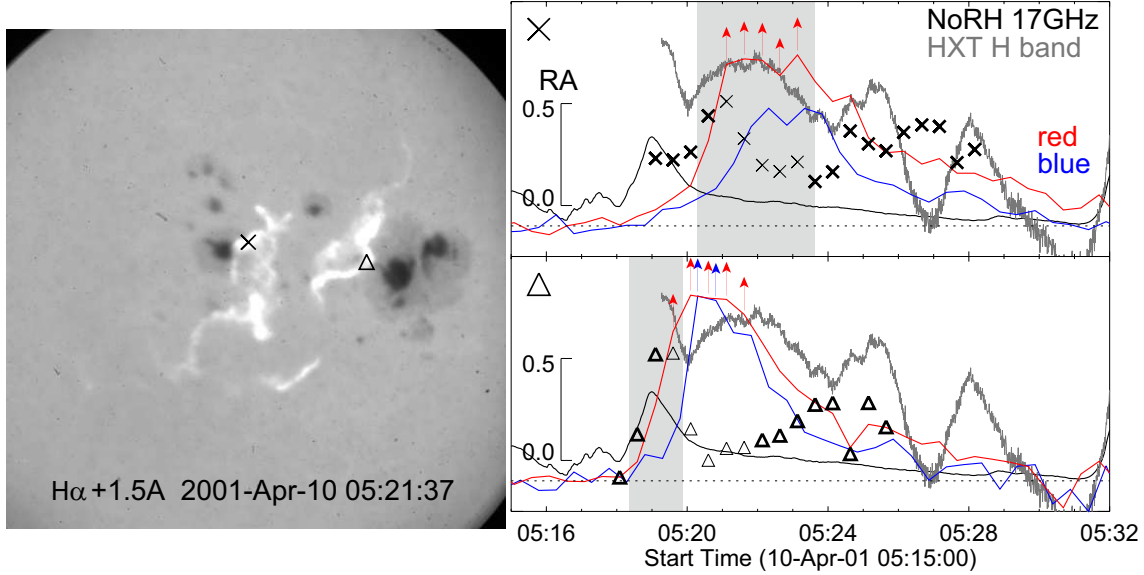


Fig. 3. Temporal evolution of $H\alpha$ kernels of the flare. The right panels show the time profiles of the $H\alpha$ kernels in the red ($+1.5 \text{ \AA}$; red line) and blue (-1.5 \AA ; blue line) wings. Microwave correlation plot observed at 17 GHz with NoRH and hard X-ray count rate measured in the H-band (53 – 93 keV) of *Yohkoh*/HXT are also plotted with the black and gray solid lines, respectively. The positions of the kernels are shown in the left panel with the cross \times and triangle Δ . Temporal evolution of RA is also over-plotted with the same (\times and Δ) signs in the right panels. The thin signs are the points calculated using the saturating intensities. Some points of the time profiles, especially the red-wing profiles, suffer from the saturation, whose intensities could be underestimated as shown with the upward arrows. The horizontal dotted lines are the zero levels of the subtracted intensities at the $H\alpha$ kernels.

gray regions in the right panels of Figure 3.

Here, we note that both I_{red} and I_{blue} are subtracted with the averaged intensity of the pre-brightening phase. Both the intensities are set to be about zero, which is shown with the horizontal dotted line in the right panels of Figure 3. In the current case, the time gaps to take images at these two wavelengths are also corrected. The $H\alpha$ red ($+1.5 \text{ \AA}$) wing images were always taken about 12 s previous to the paired blue (-1.5 \AA) wing images. To make the time profiles of red asymmetry on the right panels of Figure 3, we linearly interpolated the blue wing data so that the times correspond the observing times of the red wing data. We also have to note that the intensities are calculated by averaging the region of 5×5 pixels (which is equal to $1.''4 \times 1.''4$) around the points marked with the \times and Δ signs. These time profiles contain the region where the data suffer from the saturation, and therefore, their peaks are possibly plateaued (underestimated). We showed the points which contain such saturated data with the upward arrows in the right panels of Figure 3.

From the intensity profiles, we also obtained the temporal evolution of the red asymmetry (RA) by calculating

$$RA = \frac{I_{red} - I_{blue}}{I_{red} + I_{blue}}, \quad (1)$$

where I_{red} and I_{blue} are intensities at the red- ($+1.5 \text{ \AA}$) and blue- (-1.5 \AA) wings. The temporal evolution of RA is over-plotted with the \times and \triangle signs in the right panels of Figure 3. The data points suffering from the saturation are shown with the thin signs in the plots. These temporal evolutions of RA imply that the peaks of the red asymmetry precede those of the intensity by about 30 sec – 1 minute, while we cannot determine the exact peak times due to the saturation. Moreover, the time profiles of RA keep high values of about 0.3 – 0.4 for several minutes even after the peaks. By comparing the time profiles of RA with the microwave and hard X-ray emissions during the burst times, we found that the start times of the RA enhancements correspond with or even precede to those of the nonthermal emissions.

3.2. Spatial Distribution of RA

We examined the spatial distribution of the red asymmetry RA , by using the $H\alpha$ intensity in the red- and blue-wing images. Both I_{red} and I_{blue} are subtracted with the averaged intensity of the quiet region. The quiet region used for the analysis is the same as that used above, and is shown with the box in Figure 1 (a). We present some snap shots of the 2-dimensional RA maps to show in Figure 4. The red/blue color shows the region where red/blue asymmetry appears. We can again confirm that the red asymmetry appears all over the flare ribbons during the impulsive phase of the flare. The green-hatched regions suffer from the saturation, and therefore, we excluded them from the calculations of RA here. The temporal evolution of the RA map is also shown.

Here, we used only two wing data ($\pm 1.5 \text{ \AA}$), and we did not follow the whole line profiles, which could be strongly distorted during the flare. The RA calculated in this paper, however, can be a representative measure of the velocity, at least, at some layer of the chromosphere. Since the emission at $\pm 1.5 \text{ \AA}$ is, more or less, optically thin and is less affected from the radiative transfer effect of the vertically stratified atmospheric condensation, it serves as a simple measure of the line of sight velocity. According to $H\alpha$ profiles of flares (e.g. Ichimoto & Kurokawa 1984), RA at around $\pm 1.5 \text{ \AA}$ certainly represent the Doppler shift in line wings.

For the image taken at 05:23 UT, we also show the strong RA position ($RA \gtrsim 0.57$ and 0.65; which corresponds to more than 75 and 85 % of the maximum value of RA) on the flare ribbon with the magenta and light blue colors in the bottom right panel of Figure 4. It shows that the strong RA regions are preferentially located at the outer edge of the flare ribbons. The outer edges of flare ribbons are the footpoints of the “newly reconnected” flare loops, in the context of the magnetic reconnection model. Therefore, our result means that strong RA is associated with the footpoints of such newly reconnected loops that probably provide strong energy. The concentration of strong RA regions on the outer edges of flare ribbons is consistent with the previous works (e.g. Falchi et al. 1997). The width of the strong RA regions are about

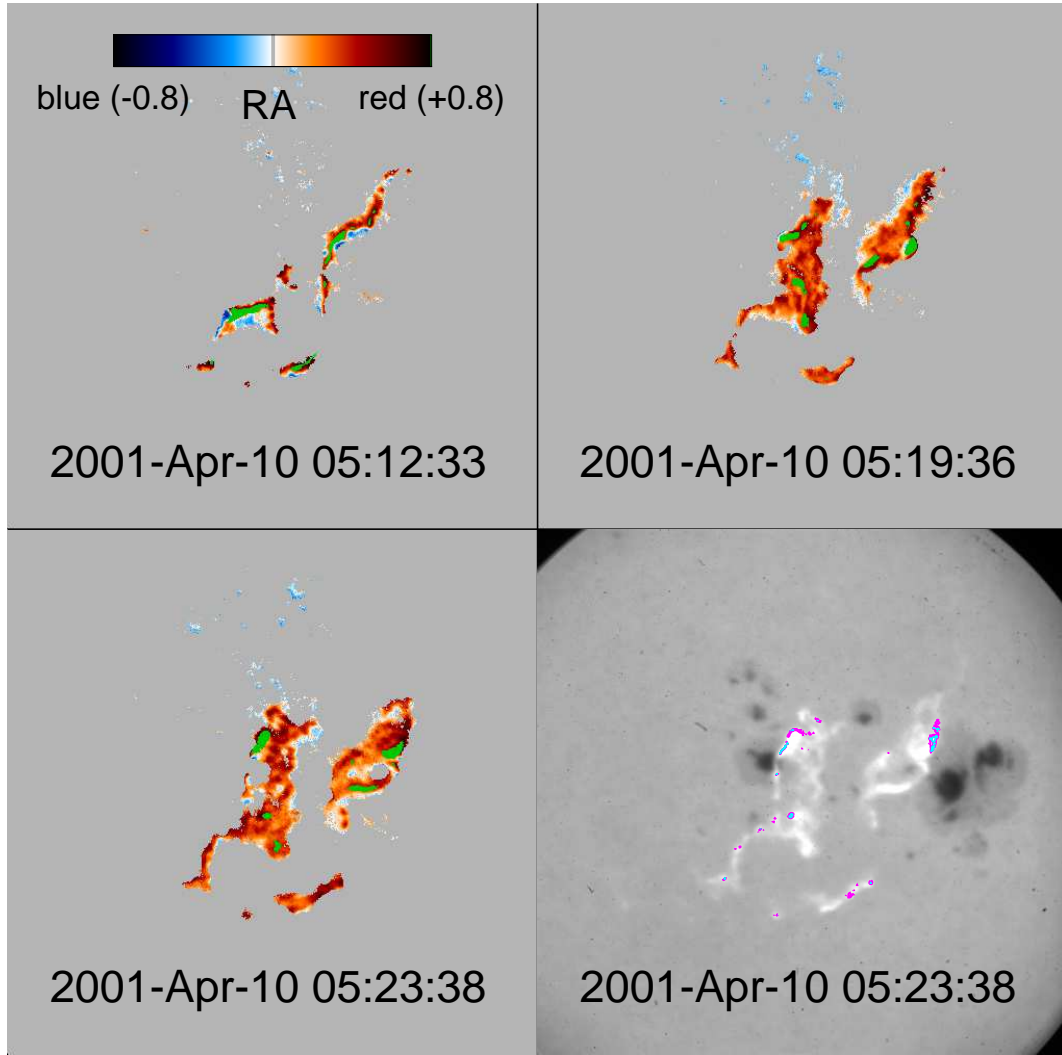


Fig. 4. Evolution of red asymmetry RA of the 2001 April 10 flare. The regions where the $H\alpha$ data suffer from the saturation are hatched with green color. The bottom right panel shows an $H\alpha$ red-wing (+1.5 Å) image overlaid with the strong RA (> 75/ > 85 %) positions with magenta/light blue colors. The times show those of the red wing data, and those for the blue wing data are delayed about 12 s from them.

1.''5 – 3.''0 (1000 – 2000 km). The length along the direction of the flare ribbons can be longer, and is about 1.''5 – 15'' (1000 – 10000 km). The largest ones are roughly consistent with the length of the hard X-ray emission sources along the flare ribbons (10'' – 20'') that appeared during the impulsive phase of the flare (Asai et al. 2004).

As we already mentioned, there is time differences between the H α red wing data and the paired blue wing data. It took about 12 s to shift the filter from the H α red (+1.5 Å) wing to the blue (−1.5 Å) wing (the red ones always precede from the blue ones in the current case). The flare ribbons expand during the flare with the speed of about 10 – 80 km s^{−1}, and even faster in the earlier phase (see Asai et al. 2004, for more detail). Therefore, the positions of the outer edges of the flare ribbons slightly different. In the current case, the flare ribbons in the blue wing data are always located outside (of about 100 – 1000 km) of those seen in the red wing data, which could cause “fake” blue asymmetry. Indeed, we can recognize the blue asymmetry in the earlier phase as seen in the top left panel of Figure 4. Although Švestka (1976) reported that such blue asymmetry sometimes appear at the earlier phase of flares, in the current case, it may be because the separation speed of the flare ribbons is much faster in the earlier phase. As the other panels of Figure 4 show, on the other hand, the time difference is not important so much in the later phase. Therefore, the RA maps in Figure 4 were made, ignoring the time differences of the 12 s. The times shown in Figure 4 are those for the red wing data.

3.3. Scatter Plot

We examined the relationship between the red asymmetry and the intensity of the H α kernels. Before this, we defined the summation (SM) and the difference (DF) of the intensities at both wings as $SM = I_{red} + I_{blue}$ and $DF = I_{red} - I_{blue}$. Therefore, the red asymmetry RA is consistent with DF divided by SM . Again, we note that I_{red} and I_{blue} are subtracted with the averaged intensity of the quiet region indicated with the rectangle in Figure 1(a).

The left panel of Figure 5 shows the scatter plot between the difference DF (horizontal axis) and the summed H α intensity SM (vertical axis) at the kernels. The “kernels” mentioned here are defined as the regions where the intensity exceeds the average intensity at the quiet region, and therefore, SM exceeds 0. We can clearly see the tendency that the stronger DF is associated with the brighter H α kernel. The regions hatched with gray color are excluded from the discussion because of the saturation.

The scatter plot shows that SM is linearly proportional to DF , that is, $SM = a \times DF (+b)$ with a proportional constant a and an intercept b . By fitting the data, we get the constant a to be about 2.5. We also confirmed that the intercept b is small (about 20 counts), and we will ignore b in the following discussion. The dark gray line in the left panel of Figure 5 is the result of the liner fitting to the data.

We also compared RA with the H α intensity SM as shown in the right panel of Figure 5.

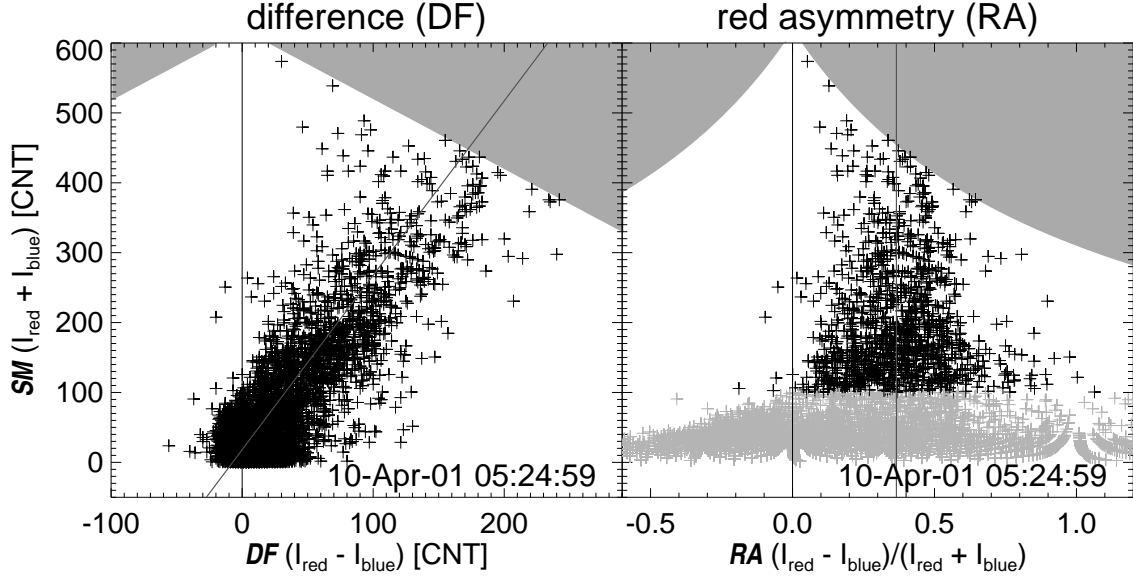


Fig. 5. Scatter plot between the red asymmetries and the intensities of the H α kernels. Left: The horizontal axis shows the difference between I_{red} and I_{blue} $DF (= I_{red} - I_{blue})$. The vertical axis shows their summed intensity $SM (= I_{red} + I_{blue})$. The dark gray line is the result of the liner fitting of the data. Right: The horizontal axis shows the red asymmetry RA , $(I_{red} - I_{blue})(I_{red} + I_{blue})^{-1} = DF/SM$. The vertical axis is the same as that of the left panel. The averaged value of the red asymmetry for the bright kernels (marked with the black signs) is shown with the vertical gray line.

The horizontal axis is RA , while the vertical axis is the same as the left panel. The regions colored gray again show the regions where the kernels suffer from the saturation. The data points seems to scatter around a mean value of 0.37 without significant correlation with intensity. By using the constant a , we can derive the relation $(I_{red} - I_{blue})(I_{red} + I_{blue})^{-1} = DF/SM = RA = a^{-1}$, and therefore, $RA = 0.4$ is expected. The mean value of the line shift at different intensity does not vary with the intensity. The averaged value of about 0.37 is calculated for the bright kernels highlighted with the black signs in the right panel of Figure 5 (that is, the data points colored with right gray are excluded for the calculation).

4. Summary and Discussions

We examined the spatially resolved red asymmetry distributions seen in the 2001 April 10 solar flare and their temporal evolution, by using the H α wing images taken with DST at Hida Observatory. We found that red asymmetry appears all over the flare ribbons, both for bright kernels generated by the bombardment of nonthermal particles and for other fainter regions generated by the (thermal) conduction. We confirmed that the strong RA appears at the outer edge of the flare ribbons that are the footpoints of newly reconnected flare loops. The width of about $1.5 - 3.0''$ ($\sim 1000 - 2000$ km). This supports that the strong energy release occurs on the magnetic loops that connect the outermost edges of the flare ribbons.

We found a clear tendency that the larger difference between the $H\alpha$ red and the blue wing intensities DF is associated with the brighter $H\alpha$ kernels SM . It turns out to be that the red asymmetry ($RA = (I_{red} - I_{blue})(I_{red} + I_{blue})^{-1} = DF/SM$) does not depend on the intensity of the $H\alpha$ kernels, and scatters around a mean value of about 0.37.

In Figure 3 we showed that the temporal evolution of RA does not synchronize with that of the intensity, and the peak times of RA time profiles precedes those of the intensities. Moreover, the enhancements of RA time profiles precede those of the nonthermal emissions observed in hard X-rays and/or in microwaves. Zarro & Canfield (1989) also mentioned that redshift in the $H\alpha$ wings starts to appear before the enhancement of the hard X-ray emission, that is, strong energy release occurs. At flare kernels, not only nonthermal particles but thermal conduction precipitate from the energy release site in the corona into the chromosphere. The preceding enhancement of RA to the hard X-ray emission could be caused by such other mechanisms rather than by nonthermal particles.

To make clear the temporal evolutions of RA and intensity, we overlaid the temporal trajectories of the $H\alpha$ kernels, shown in Figure 3 with the \times and \triangle signs, on the scatter plot between RA and the summed intensity SM , which is presented as Figure 6. The RA plots move counter-clockwise on the scatter plot, and after the RA enhancements, the intensities reach the peak. The absence of a clear correlation with the intensity is because the time profile of RA for individual kernels evolves independently with a manner that the peak downward velocity is not a strong function of their peak intensity. Canfield et al. (1990) also reported that there is no one-to-one relation between brightness of $H\alpha$ line center and redshift, while they found many redshift features at bright kernels at $H\alpha$ line center.

If we assume a constant width of the $H\alpha$ emission line, we can regard RA as an indicator of the velocity. For example, assuming a gaussian function with the full-width-half-maximum $FWHM$ in \AA , RA can be related to the Doppler (redward) velocity as $2.75 \times \ln(1 + RA)(1 - RA)^{-1}(FWHM(\text{\AA}))^2 \text{ km s}^{-1}$. The estimation of the width of the $H\alpha$ emission line is, however, very difficult, because the shape of the line is drastically changed (it cannot be fitted with a gaussian function) and especially the Stark effect broadens the line at the wings (Švestka 1976). From the results of Ichimoto & Kurokawa (1984) (in the Figs. 3b and 4b), we estimated RA for their flares, and they are about 0.2 – 0.5, which is comparable to the 2001 April 10 flare. They also reported that the Doppler velocities are 10 – 100 km s^{-1} , the $FWHM$ of about 4.5 – 6.0 is expected. If we assume that the $FWHM$ is about 5.0, here, RA of 0.37 turns out the Doppler (downward) velocity of about 53 km s^{-1} . Scattering of RA around a certain value of about 0.37 is also because the time profiles of RA keep high values for several minutes even after the intensity peaks. This means that the downward motion at flare ribbons continues with the velocity of about several tens of km s^{-1} independently from the intensity.

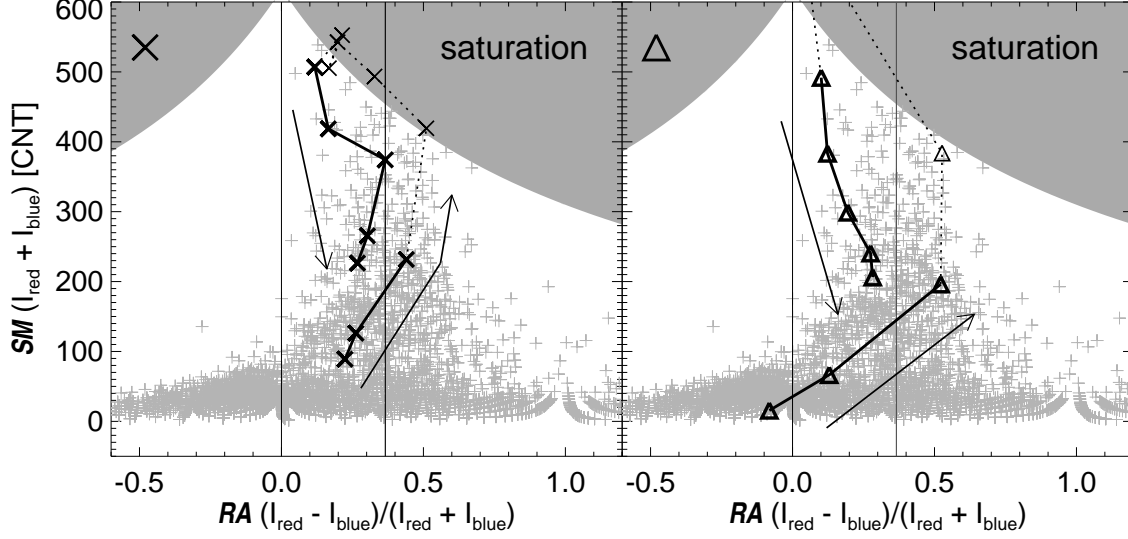


Fig. 6. Temporal trajectories of H α kernels in the $RA - SM$ scatter plot. The temporal evolutions of RA are shown in the right panels of Figure 3, and the marks of the H α kernels (cross \times and triangle \triangle signs) are also the same as those shown in Figure 3. The arrows guides the temporal evolutions. The background $RA - SM$ scatter plots are the same as the right panel of Figure 5.

Acknowledgements

We first acknowledge an anonymous referee for her/his useful comments and criticisms. This work was supported by the Grant-in-Aid for the Global COE Program “The Next Generation of Physics, Spun from Universality and Emergence” from the Ministry of Education, Culture, Sports, Science and Technology (MEXT) of Japan.

References

- Antonucci, E., Gabriel, A. H., Dennis, B. R. 1984, *ApJ*, 287, 917
- Asai, A., Masuda, S., Yokoyama, T., Shimojo, M., Isobe, H., Kurokawa, H., and Shibata, K. 2002, *ApJ*, 578, L91
- Asai, A., Ishii, T.T., Kurokawa, H., Yokoyama, T., and Shimojo, M. 2003, *ApJ*, 586, 624
- Asai, A., Yokoyama, T., Shimojo, M., Masuda, S., Kurokawa, H., and Shibata, K. 2004, *ApJ*, 611, 557
- Canfield, R. C., Kiplinger, A. L., Penn, M. J., Wülser, J.-P. 1990, *ApJ*, 363, 318
- Carmichael, H. 1964, in *The Physics of Solar Flares*, ed. W. N. Hess (NASA SP-50), 450
- Domingo, V., Fleck, B., Poland, A. I. 1995, *Sol. Phys.*, 162, 1
- Falchi, A., Qiu, J., Cauzzi, G. 1997, *A&A*, 328, 371
- Fisher, G. H., Canfield, R. C., McClymont, A. N. 1985a, *ApJ*, 289, 414
- Fisher, G. H., Canfield, R. C., McClymont, A. N. 1985b, *ApJ*, 289, 425
- Hanaoka, Y. 2003, *ApJ*, 596, 1347
- Hirayama, T. 1974, *Sol. Phys.*, 34, 323

- Ichimoto, K., & Kurokawa, H. 1984, *Sol. Phys.*, 93, 105
- Janssens, T. J., & White, K. P. III 1970, *Sol. Phys.*, 11, 299
- Kopp, R. A., & Pneuman, G. W. 1976, *Sol. Phys.*, 50, 85
- Kosugi, T., et al. 1991, *Sol. Phys.*, 136, 17
- Nakajima, H., et al. 1994, *Proc. of IEEE*, 82, 705
- Ogawara, Y., Takano, T., Kato, T., Kosugi, T., Tsuneta, S., Watanabe, T., Kondo, I., & Uchida, U. 1991, *Sol. Phys.*, 136, 1
- Okamoto, T. J., Nakai, H., Keiyama, A., Narukage, N., UeNo, S., Kitai, R., Kurokawa, H., Shibata, K. 2004, *ApJ*, 608, 1124
- Sturrock, P. A. 1966, *Nature*, 211, 695
- Sturrock, P. A. 1992, in *IAU Colloq. 133, Eruptive Solar Flares*, ed. Z. Švestka, B. V. Jackson, & M. E. Machado (New York: Springer), 397
- Švestka, Z. 1976, *Solar Flares* (Dordrecht: Reidel) 55
- Švestka, Z., & Cliver, E. W. 1992, in *IAU Colloq. 133, Eruptive Solar Flares*, ed. Z. Švestka, B. V. Jackson, & M. E. Machado (New York: Springer), 1
- Tandberg-Hanssen, E. & Emslie, A. G. 1988, *The Physics of Solar Flares* (Cambridge: Cambridge University Press)
- Tang, F. 1983, *Sol. Phys.*, 83, 15
- Xie, W., Zhang, H., Wang, H. 2009, *Sol. Phys.*, 254, 271
- Zarro, D. M., Canfield, R. C. 1989, *ApJ*, 338, L33